Electrochemically Synthesized Polyaniline Nanofibers on Flexible Electrode for pH Sensing

Electroanalysis

ELECTROANALYSIS
An International Journal Devoted to Electroanalysis, Sensors and Bioelectronic Devices

RESEARCH ARTICLE OPEN ACCESS

Electrochemically Synthesized Polyaniline Nanofibers on Flexible Electrode for pH Sensing

Jian Zhang[1] | Mostafa Salehirozveh[1] | Shadi Rahimi[1] | Erik Gerner[2] | Santosh Pandit[1] | Ivan Mijakovic[1,3]

[1]Systems and Synthetic Biology Division, Department of Life Sciences, Chalmers University of Technology, Gothenburg, Sweden | [2]Mölnlycke Health Care AB, Gothenburg, Sweden | [3]The Novo Nordisk Foundation, Center for Biosustainability, Technical University of Denmark, Kongens Lyngby, Denmark

Correspondence: Ivan Mijakovic (ivan.mijakovic@chalmers.se)

Received: 12 November 2025 | **Revised:** 7 January 2026 | **Accepted:** 10 January 2026

Keywords: drift rate | electrochemical deposition | pH sensor | polyaniline nanofibers | wound monitoring

ABSTRACT

pH monitoring is essential in diverse fields such as clinical diagnostics, environmental surveillance, food quality control, and industrial process management. Wound exudate pH serves as a noninvasive biomarker of wound status. Here, we report a flexible electrochemical pH sensor based on polyaniline nanofiber (PANI NF) modified polyimide electrodes prepared by electrochemical deposition. The nanofibrous PANI layer exhibits a porous interconnected architecture, as confirmed by scanning electron microscope (SEM), Fourier transform infrared (FTIR), Raman, and X-ray photoelectron spectroscopy (XPS) analyses. The PANI NF electrode displayed a near-Nernstian sensitivity of 57 mV pH^{-1} over the pH 5–9 range with excellent linearity ($R^2 > 0.99$), low hysteresis (<4 mV), and high reproducibility (RSD 0.54%). Long-term drift studies revealed minimal potential drift (<1 mV h^{-1}), and the calibration slope remained unchanged after 5 days of floating. The sensor accurately measured the pH of serum-containing simulated wound fluid (SWF), with deviations ≤ 0.06 from a commercial glass-electrode pH meter. After 90 days of storage at 4°C in the dark, the sensor retained its sensitivity with only minor variability (RSD 2.77%). These results demonstrate that the flexible PANI based sensor offers fast response, high sensitivity, and excellent stability, making it a promising platform for real-time, continuous monitoring of wound exudate pH and other biomedical or environmental applications.

1 | Introduction

pH measurement is a fundamental analytical task in diverse fields including clinical diagnostics, environmental monitoring, food quality control, and industrial process management [1, 2]. For example, the wound healing process is a complex and dynamic cascade involving hemostasis, inflammation, proliferation, and remodeling. Monitoring the pH of wound exudate has become a vital, noninvasive method for evaluating wound status and guiding timely clinical decisions [3]. Healthy, healing wounds generally progress toward a slightly acidic environment, which supports optimal enzymatic activity, encourages fibroblast, and keratinocyte function, and helps to suppress the bacterial proliferation. In contrast, chronic or infected wounds often maintain an alkaline pH, signaling impaired healing, elevated protease activity, and microbial colonization [4, 5]. Thus, continuous pH monitoring can facilitate early detection of wound deterioration and enhance patient outcomes [6].

Flexible electronics and electronic skin technologies offer a promising strategy, as mechanically compliant electrodes can conform closely to wound surfaces, enabling long-term, noninvasive, real-time monitoring of wound exudate pH [7, 8]. Such systems are biocompatible, scalable, and readily integrated into wearable platforms, offering significant potential for personalized wound care and early detection of complications. Flexible polymer substrates are widely used for skin-conformable sensors due to their ease of surface modification, which facilitates the development of conductive electrodes [9]. Conductive polymers, with tunable electrical properties, chemical stability, and processability, can transduce chemical or biological signals into measurable electrical changes [10]. Among them, polyaniline

(PANI) is particularly attractive for pH sensing due to its reversible protonation and deprotonation, which cause measurable changes in conductivity in response to ambient pH. Incorporating PANI into polymer substrates enables flexible, wearable, real-time pH sensors suitable for biomedical applications such as wound monitoring [11, 12]. PANI thin films can be fabricated via various techniques, including electrochemical polymerization, in situ chemical polymerization, spray and drop coating, plasma polymerization, and spin coating methods [13]. Electrochemical deposition is especially advantageous for its simplicity, scalability, and rapidity, while also enabling the formation of nanostructured PANI—such as nanofibers (NFs)—which provide high surface area, rapid ion transport, and short diffusion paths. These nanostructured electrodes have demonstrated excellent performance in diverse electrochemical devices, highlighting their potential in wearable pH sensing [14–16].

Electrochemical deposition of PANI NF represents a significant methodological advancement in electrochemical pH sensing. In this study, we developed an electrochemical pH sensor based on a PANI NF modified polymer electrode. A layer of PANI NFs was electrochemically deposited onto a polyimide (PI) substrate coated with a thin gold film. The surface properties of the PANI NF electrode were characterized using a range of spectroscopic techniques. The electrode was evaluated using open-circuit potential (OCP) measurements in buffer solutions with pH ranging from 5 to 9. The PANI NF electrode exhibited excellent sensitivity and reproducibility. Long-term signal stability is a critical concern for PANI-based pH sensors due to potential signal drift. To explore this issue, we evaluated the drift of the PANI NF electrode by performing continuous OCP measurement in buffer for 24 h and potentiometric measurement after 24 h of floating in PBS. The results showed minimal drift, stable performance, and no sensitivity loss over time. Furthermore, pH measurements in simulated wound fluid (SWF) confirmed the sensor's accuracy in a biologically relevant environment, highlighting its potential for real-time, continuous wound monitoring.

2 | Experimental Section

2.1 | Chemicals and Materials

Sodium dihydrogen phosphate monohydrate ($NaH_2PO_4{\cdot}H_2O$), disodium hydrogen phosphate heptahydrate ($Na_2HPO_4{\cdot}7H_2O$), aniline, sulfuric acid (H_2SO_4), potassium chloride (KCl), and PI substrates with a thickness of 125 μm were all purchased from Sigma-Aldrich (Sweden). SWF (50% heat-inactivated fetal bovine serum in maximum recovery diluent) and modified SWF (34 g/L BSA in a buffered salt solution, Table S1) were purchased from Sahlgrenska substrate service (Sweden) [17]. The studies used ultrapure Millipore water with a resistivity of 18.2 MΩ cm.

2.2 | Preparation of PI/PANI NF Electrodes

PI substrates were first sonicated in acetone for 15 min to remove debris and surface contaminants. The cleaned substrates were subsequently rinsed with ethanol and deionized water, followed by complete drying under a nitrogen stream. A Cr/Au bilayer (5/100 nm) was uniformly deposited on the PI surface via thermal evaporation to yield PI/Au electrodes. Electrochemical polymerization of PANI NF was performed in a three-electrode electrochemical workstation. The PI/Au electrodes were encapsulated with an inert insulating polymer, leaving a fixed exposed area of $1 \times 1\ cm^2$ in contact with the electrolyte as a working electrode. The electrolyte consisted of a homogeneous, transparent, light-yellow solution prepared from 60 mM aniline and 0.5 M H_2SO_4. Cyclic voltammetry (CV) was carried out between −0.2 and 1.0 V at a scan rate of 0.1 V/s for 20 cycles. After polymerization, the resulting PI/PANI electrodes were thoroughly rinsed with deionized water to remove residual ions and dried at room temperature.

2.3 | Characterization

The PI/PANI NF was observed using a field-emission scanning electron microscope (SEM, FESEM, JEOL 7800F Prime) at an accelerating voltage of 5 kV. Fourier transform infrared (FTIR) spectra were collected with a Vertex 70v Bruker Alpha spectrometer in attenuated total reflectance (ATR) mode using a diamond crystal, with each spectrum obtained by averaging 256 scans at a resolution of $4\ cm^{-1}$. Raman spectra were recorded on a WITec alpha300 confocal Raman spectrometer equipped with a 100× objective, a 532 nm excitation laser, and a 600 g/mm grating, over the 200–3600 cm^{-1} range with an integration time of 0.5 s. Surface chemical compositions were analyzed using X-ray photoelectron spectroscopy (XPS, PHI VersaProbe III) with monochromated Al Kα radiation (1486.6 eV), and the spectra were processed using CasaXPS software.

2.4 | Electrochemical Experiment

CV, electrochemical impedance spectroscopy (EIS), and OCP measurements were conducted using a CHI6048E electrochemical workstation. A three-electrode system was employed, with Ag/AgCl (saturated KCl) as a reference electrode, a Pt wire as a counter electrode, and the PANI NF electrode as a working electrode. Buffer solutions with pH values ranging from 5 to 9 were prepared using $NaH_2PO_4{\cdot}H_2O$ and disodium hydrogen phosphate. For each pH value, the potential was recorded over 250 s at room temperature (22 ± 1°C) to assess the sensitivity of the sensor. The potential change can be used to measure the reversibility of the sensor. In this study, the prepared PANI sensor was immersed in a buffer solution with a pH of 5–9 for reciprocating cycling tests. The OCP of the PI/PANI NF sensor was then continuously measured for 24 h in buffer solutions. The change in OCP over 24 h was used as a criterion for the sensor drift rate ($mV\ h^{-1}$). In addition, the OCP of the PI/PANI NF sensors was measured after floating in buffer solutions with different pH values for 24 h.

3 | Results and Discussion

3.1 | Characterization of the Structure and Morphology of PANI

The surface morphology, chemical composition, and molecular structure of the prepared PANI NF electrodes were examined using SEM, FTIR, XPS, and Raman spectroscopy. The PI substrate covered with gold has a smooth and flat surface, as shown

in Figure S1. The SEM images of electrochemically deposited PANI film exhibit a uniform nanofibrous network with an average fiber diameter of about 100 nm, forming a porous and interconnected architecture (Figure 1A,B). Such a structure provides a large surface area and abundant electrochemical active sites, thereby facilitating charge transfer and ion diffusion in electrochemical applications. The molecular vibration features of the prepared PANI were characterized by FTIR spectroscopy (Figure 1C). The absorption bands at about 1560 and 1480 cm^{-1} correspond to the stretching vibrations of quinoid and benzenoid rings, respectively, confirming the characteristic backbone of PANI. The peak at 1300 cm^{-1} is attributed to C—N stretching within the benzenoid units, while the band at 1140 cm^{-1} is associated with vibrations of protonated structures, indicative of the conducting emeraldine salt form. In addition, the absorption peak at 800 cm^{-1} originates from out-of-plane bending of C—H bonds in the aromatic rings [18, 19]. These results verify the successful formation of PANI with typical structural features. The surface chemical composition of PANI was further analyzed by XPS (Figure 1D). The survey spectrum confirmed the presence of C, N, and O, consistent with the expected polymer composition. High-resolution C1s spectra (Figure 1E) revealed six main components: the dominant peak at 284.6 eV assigned to sp^2-hybridized C═C/C—C bonds in the aromatic rings, a component at 285.5 eV corresponding to sp^3-hybridized C—C/C—H bonds arising from structural disorder, a peak at 286.2 eV attributed to C—N and/or C—O bonds, and peaks at 287 and 288.2 eV associated with C═O and O—C═O groups, likely introduced by air exposure or partial electrochemical oxidation. At higher binding energy, a weak shakeup satellite peak was observed, originating from π–π transitions in the conjugated aromatic system, further supporting the extended conjugation of the PANI backbone [20, 21]. The high-resolution N1s spectrum was deconvoluted into three components: imine (═N—, 398.5 eV), amine (—NH—, 399.5 eV), and protonated amine ($—NH^+$, 401.3 eV), confirming the emeraldine salt state (Figure 1F) [18, 22]. In the Raman spectrum of PANI, several characteristic bands can be clearly identified (Figure S2). The peaks at 1404, 1483, and 1606 cm^{-1} correspond to the C—C stretching, C═N stretching, and C═C stretching vibrations of the quinoid rings, respectively. In addition, the band observed at 1230 cm^{-1} is assigned to the C—N stretching vibration of the benzenoid structure, while the band at 1166 cm^{-1} is attributed to the in-plane C—H bending vibration of the quinoid unit. Another noticeable band appears at 816 cm^{-1}, which is associated with the out-of-plane C—H bending vibration. These vibrational features confirm the coexistence of both benzenoid and quinoid structural units within the PANI backbone [23].

3.2 | Evaluation of the Electrochemical Behavior of PANI-Based Sensor

The electrochemical synthesis of PANI NF was performed by electropolymerization using CV (Figure S3). As shown in Figure 2A, the CV curves display characteristic redox peaks during deposition, corresponding to the successive transitions between leucoemeraldine, emeraldine, and pernigraniline states, indicating the gradual growth of a PANI film on the electrode surface. Both anodic and cathodic peak currents increase with the number of CV cycles, reflecting the progressive formation and increasing coverage of the PANI [15, 24]. The electrochemical behavior of the PANI NF electrode was further evaluated in the $[Fe(CN)_6]^{3-/4-}$ redox probe. Compared to the bare electrode, the CV of PANI NF electrode exhibited a larger redox potential separation, decreased peak currents, and reduced reversibility, indicating slower charge transfer kinetics due to the presence of the PANI layer (Figure 2B). EIS was employed to evaluate

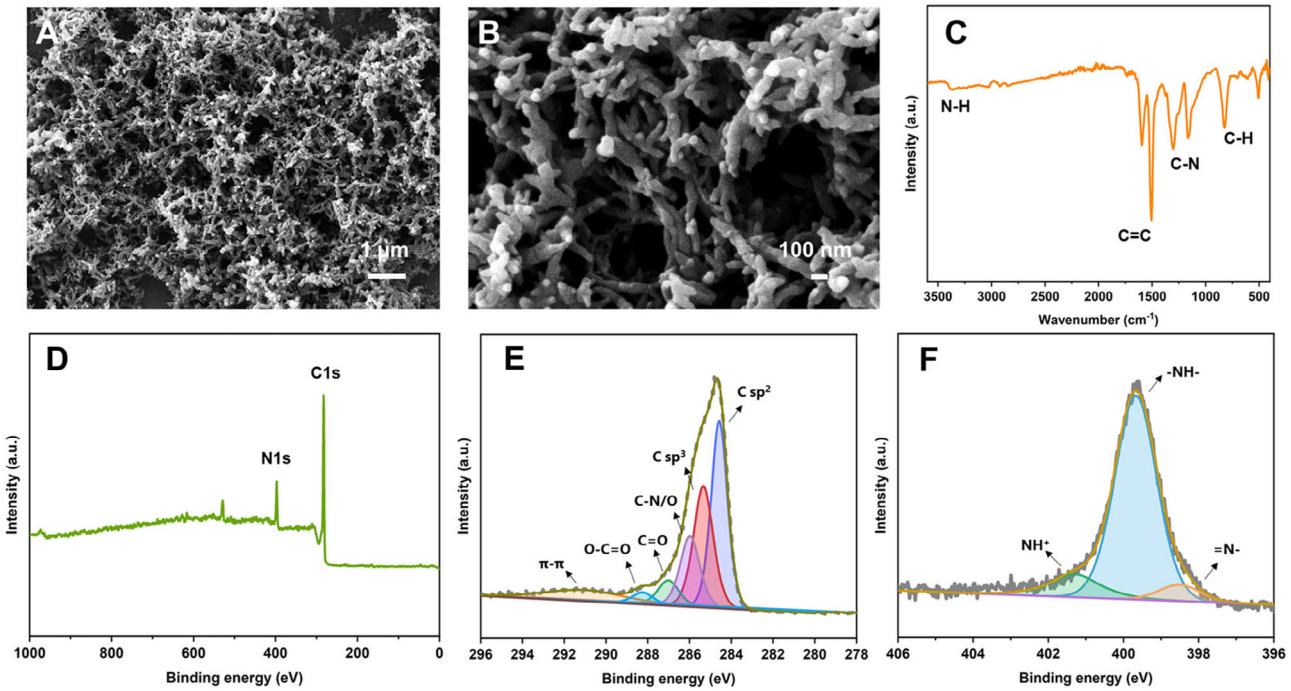

FIGURE 1 | SEM images of PANI nanofiber films (A,B), FTIR spectrum (C), XPS survey spectrum (D), and high-resolution C 1s (E) and N 1s (F) spectra.

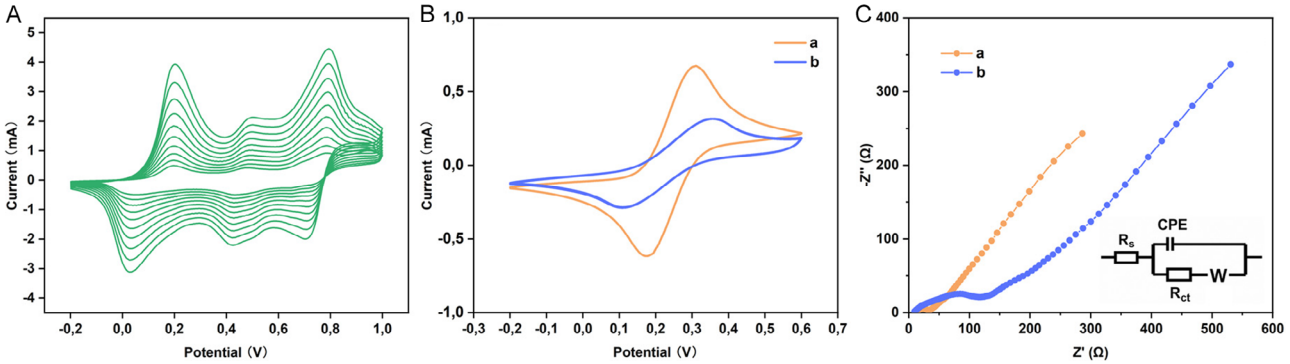

FIGURE 2 | (A) CV curves during PANI deposition on the bare electrode in a solution of 60 mM aniline and 0.5 M H_2SO_4 at a scan rate of 100 mV/s. (B) CV curves and (C) Nyquist plots of the bare electrode (a) and the PANI NF electrode (b), both recorded in 0.01 M PBS containing 5 mM $K_3[Fe(CN)_6]$/$K_4[Fe(CN)_6]$ and 0.1 M KCl. The inset in (C) shows the equivalent circuit used to fit the impedance data.

the interfacial properties of the bare and PANI NF electrodes (Figure 2C). An equivalent circuit was used to fit the experimental EIS data, as shown in the inset of Figure 2C. In this circuit, R_s represents the solution resistance, R_{ct} denotes the charge transfer resistance at the electrode–electrolyte interface, W corresponds to the Warburg impedance associated with diffusion processes, and the constant phase element (CPE) accounts for the nonideal double-layer capacitance. The fitted results reveal that the R_{ct} value of the PANI NF electrode (128 Ω, curve b) is higher than that of the bare electrode (28 Ω, curve a), indicating the formation of a PANI film on the electrode surface that partially hinders charge transfer between the redox probe and the electrode. The decreased peak current and increased impedance suggest that, although the PANI NF provides additional electroactive sites, its intrinsic resistance impedes electron transfer of the $[Fe(CN)_6]^{3-/4-}$ redox couple, consistent with previous reports [25].

The electrochemically active surface area (ECSA) was calculated using the Randles–Sevcik equation:

$$I_p = 2.69 \times 10^5 A D^{1/2} n^{3/2} r^{1/2} C$$

where n is the number of electrons participating in the reaction, D is the diffusion coefficient of the molecule (7.6×10^{-6} cm^2 s^{-1}), A is the electroactive surface area, C is the concentration of analyte (mol cm^{-3}), and r is the scan rate (V s^{-1}) [26]. The calculated ECSA of the bare electrode and PANI NF electrode were about 0.74 and 0.35 cm^2, respectively. Despite the high surface area of the PANI NF electrode's network structure, its measured ECSA is smaller than that of the bare electrode. This is likely due to the relatively large size of the $[Fe(CN)_6]^{3-/4-}$ probe, which may not effectively penetrate the PANI matrix, resulting in a lower observed ECSA. Additionally, the porous structure of PANI creates complex diffusion pathways for ions and probe molecules, and the increased path length further hinders their transport to the electroactive sites [27, 28].

The sensing mechanism of the PANI pH sensor is based on the reversible protonation and deprotonation of PANI in different pH environments (Figure 3). In acidic solutions, PANI is protonated to form the highly conductive emeraldine salt, which decreases the surface resistance of the sensor and leads to a change in the OCP. In alkaline solutions, the protons associated with PANI are neutralized by OH^-, converting it to the less

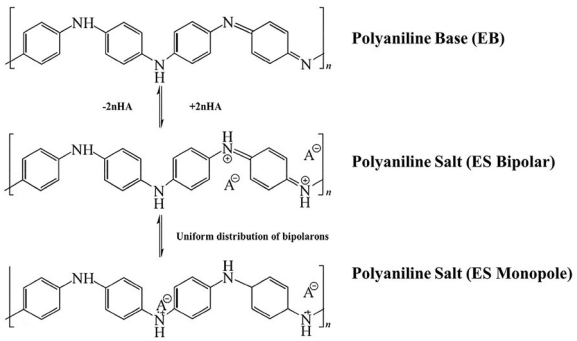

FIGURE 3 | Scheme of the protonation–deprotonation mechanism for PANI.

conductive emeraldine base, which increases the resistance and produces an opposite potential response compared to acidic conditions. According to the Nernst equation, the OCP can be expressed as $E = E_0 + 0.0591 \times \text{pH}$ (V), reflecting a linear dependence on pH. This reversible protonation–deprotonation process enables the PANI sensor to respond sensitively to different pH values [9, 11, 16].

3.3 | The Electroanalytical Sensing of pH

The OCP response of the PANI sensor was examined under varying pH conditions. As shown in Figure 4A, the potential shifted systematically with increasing pH, which can be attributed to the protonation–deprotonation transition of the PANI backbone from the emeraldine salt to the emeraldine base state. Plotting the equilibrium potential values against pH in the range of 5.0–9.0 (Figure 4B) yielded a highly linear relationship, with a slope of 57 mV pH^{-1} and a correlation coefficient (R^2 0.99). These results are in close agreement with the theoretical Nernstian response, confirming that the redox-active sites of PANI enable efficient and reproducible transduction of H^+ activity. Moreover, the relative standard deviation (RSD, $n = 5$) of the PANI sensor's sensitivity was 0.54%, demonstrating that the PANI sensor exhibits excellent reproducibility for pH detection. The electrochemical potential of the PANI pH sensor can vary during repeated measurements. This phenomenon, known as potential hysteresis or "memory effect," reflects the reversibility of the sensor [28]. To evaluate its reversibility, the same sensor

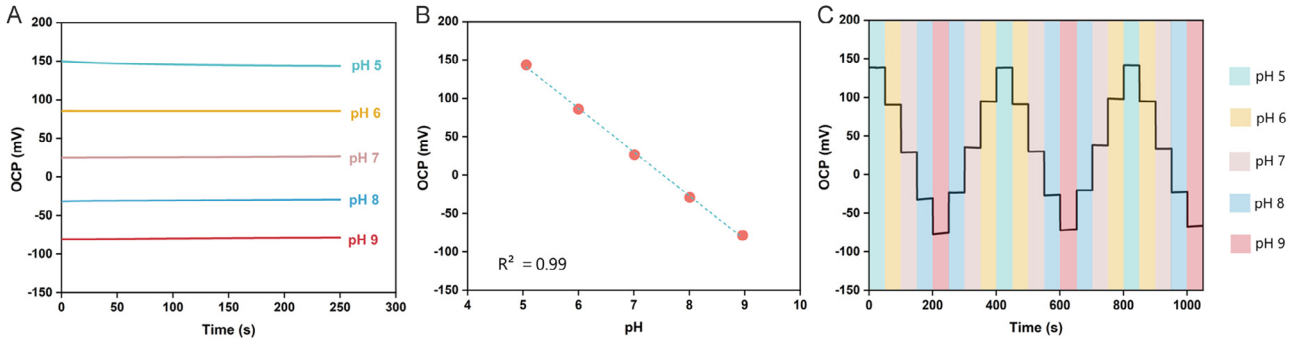

FIGURE 4 | Open-circuit potential (OCP) curves of the PANI sensor (A); linear relationship between potential and pH in the range of 5.0–9.0 (B); and reversibility evaluation of the PANI sensor over the pH 5.0–9.0 range (C).

was subjected to cycling measurements over a pH range of 5.0–9.0 (Figure 4C). The OCP values at each pH plateau remained highly stable throughout successive cycles. The hysteresis width, defined as the potential difference between forward and backward sweeps, was minimal, remaining below 4 mV across the tested range. Repeatability was evaluated by analyzing potential variations at each pH over three consecutive cycles, with RSD values ranging from 1.0% to 4.4%, demonstrating excellent consistency under repeated use. Collectively, the small hysteresis potentials and low RSD values confirm that the PANI-based sensor possesses outstanding reversibility and repeatability within the physiologically relevant pH range of 5.0–9.0.

The response time of the prepared PANI pH sensor was evaluated by exposing it to a step change in buffer pH. The response time was defined as the period required for the initial potential to reach 90% of the equilibrium potential [29, 30]. Figure 5A shows the sensor's response to a step change from pH 7.0 to pH 5.0. The measured response time of the PANI sensor was 10.5 s, confirming its rapid pH response and showing good agreement with values reported for other PANI-based electrodes in the literature [9, 30]. In addition to evaluating the sensitivity of the PANI-based pH sensor, its long-term stability is also of great importance for practical applications. Therefore, the drift behavior of the PANI sensor was investigated to assess its reliability under continuous operation [18, 31]. To evaluate the long-term stability and drift characteristics of PANI electrodes, the study compared two different testing methods. In the first method, the electrode was sequentially measured in different buffer solutions for 24 h to simulate continuous operation under varying pH conditions. As shown in Figure 5B, the sensor exhibited very low potential drift during continuous measurement, with rates of 0.73 mV h^{-1} at pH 5.0, 0.82 mV h^{-1} at pH 6.0, 0.58 mV h^{-1} at pH 7.0,

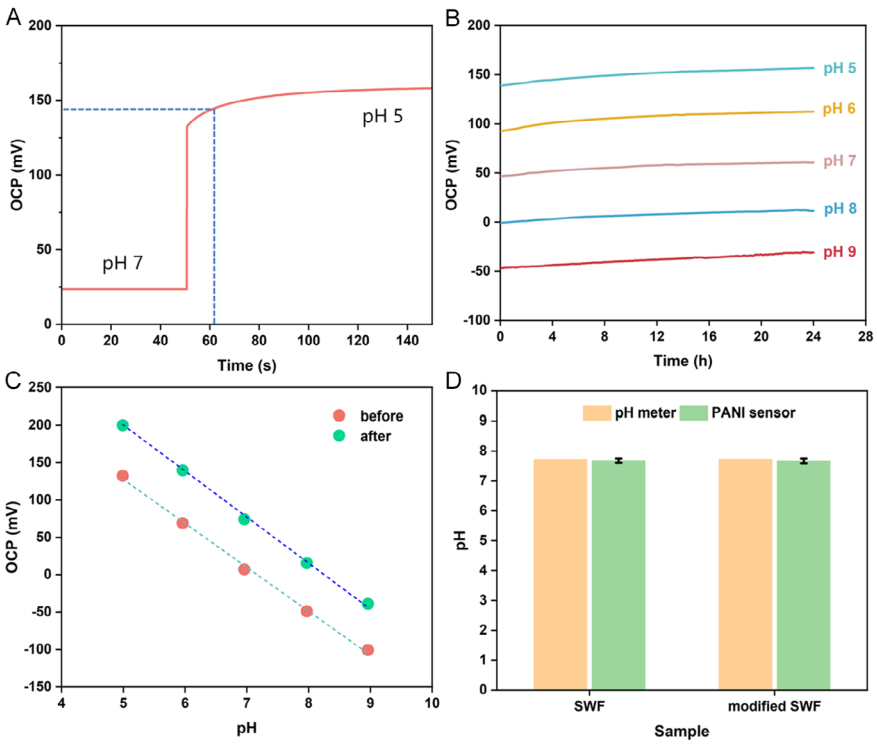

FIGURE 5 | (A) Temporal response from pH 7.0 to pH 5.0 for PANI sensor. (B) The OCP drift of the PANI sensor during 24 h of continuous measurement at pH 5–9. (C) Linear relationship between potential and pH before and after 5 days of immersion at pH 5.0–9.0. (D) Practical application of the PANI pH sensor for monitoring the pH of SWF and modified SWF.

$0.53\ mV\ h^{-1}$ at pH 8.0, and $0.68\ mV\ h^{-1}$ at pH 9.0. All drift rates are less than $1\ mV\ h^{-1}$. It should be noted that the OCP drift measurements were conducted sequentially using the same electrode; therefore, the initial OCP at each pH reflects the cumulative drift from previous long-term measurements, resulting in systematically higher initial OCP values. In the second method, the electrode was immersed in each buffer solution for 24 h and subsequently measured under OCP conditions, aiming to evaluate the electrode response after long-term equilibration in a single pH environment. The results showed that the drift values obtained by the two methods were highly consistent (Table S2). This suggests that the observed drift mainly originates from the intrinsic redox and protonation–deprotonation equilibria within the PANI, rather than from external factors introduced by sequential measurements or solution exchange during the test. In addition, the OCP was measured after PANI electrode had been immersed in buffer solutions with pH values from 5.0 to 9.0 for 5 days, and calibration curves were generated (Figure 5C). Although the OCP values at each pH increased, the slope of the calibration curve remained essentially unchanged. This demonstrates that the pH sensitivity and linear response of the PANI electrode were preserved, and the drift manifested mainly as a uniform potential shift. Such shifts can be corrected through routine calibration without compromising analytical performance, which is advantageous for both continuous and intermittent pH monitoring. Collectively, these findings show that the PANI pH sensor combines a fast response with excellent long-term stability. To evaluate the applicability of the prepared PANI pH sensor for biomedical environments, the pH values of SWF and modified SWF were measured and compared with those obtained using a commercial glass-membrane pH meter. SWF was prepared by mixing equal volumes of 0.9% NaCl containing 0.1% peptone water (PW) and foetal bovine serum (FBS), resulting in a final composition of 50% PW and 50% FBS, which mimics the high protein content of chronic wound exudate. Modified SWF, based on bovine serum albumin as a protein source, represents an alternative but more reproducible simulated wound media [17]. As shown in Figure 5D, the pH values measured using the PANI sensor were consistent with those measured using a commercial meter. The pH values of the SWF and modified SWF measured by the PANI sensor were 7.68 and 7.67, respectively, while the pH values obtained using the commercial pH meter were 7.72 and 7.73, respectively. The deviations for both methods were no more than 0.06, demonstrating that the PANI sensor possesses high accuracy comparable to that of the widely used commercial pH electrodes in both albumin- and the more complex serum-based test media. Furthermore, due to its flexibility, the PANI sensor has the potential to directly measure the pH of SWF droplets placed on irregular or curved substrates, a feat not possible with conventional glass electrodes. These results demonstrate the potential of the PANI sensor for pH monitoring in a simulated wound environment and provide a promising platform for future applications in wound care prognosis. In addition, the lifetime of the PANI sensor was also evaluated. After 90 days of storage at 4°C in the dark, the sensor retained its sensitivity with minimal change over time, exhibiting an RSD of 2.77%. A comparative study of PANI-based pH electrochemical sensors was conducted to evaluate their performance characteristics, as summarized in Table S3. The developed sensor exhibited a near-Nernstian sensitivity of $57\ mV\ pH^{-1}$, which is very close to the theoretical value of $59\ mV\ pH^{-1}$ in the pH range of 5–9. Evaluating sensor performance under more stringent and physiologically relevant conditions is of great importance, for example, in media such as human serum that mimic the chemical environment near wound sites [32]. In this study, the PANI-based pH sensor was validated in SWF to emulate a more realistic wound environment. The measured pH values showed deviations of less than 0.06 pH units compared with those obtained using a commercial glass electrode, demonstrating high measurement accuracy and confirming the reliable performance of the PANI sensor in biofluid-like media, which is essential for wound monitoring applications. Moreover, the PANI sensor maintained excellent stability after 90 days of storage at 4°C, with only a minor change in sensitivity (RSD = 2.77%). These results indicate that the developed sensor possesses both high analytical reliability and long-term durability, highlighting its potential for practical and translational use.

4 | Conclusions

A flexible pH sensor based on electrochemically deposited PANI NFs on a PI substrate was successfully fabricated and comprehensively characterized. The nanofibrous PANI network provided abundant active sites, enabling a near-Nernstian response ($57\ mV\ pH^{-1}$) over the physiological pH range with high reproducibility and minimal hysteresis. Long-term drift studies confirmed that the sensor maintained stable calibration slopes and very low potential drift both during continuous measurement and after immersion in buffer solutions. The sensor also delivered accurate pH readings in protein-rich SWF, comparable to those of a commercial glass-electrode pH meter, and retained its sensitivity after 90 days of storage at 4°C. These findings indicate that the proposed PANI-based sensor combines high sensitivity, and robust stability. In future work, the developed PANI based pH sensor could be integrated into wound dressings to enable continuous and noninvasive monitoring of wound healing and infection status.

Acknowledgments

This study was supported by the VINNOVA (2022–03813) and 2D TECH VINNOVA competence center (2019-00068).

Funding

This study was supported by the VINNOVA (2022–03813) and 2D TECH VINNOVA (2019-00068).

Conflicts of Interest

The authors declare no conflicts of interest.

Data Availability Statement

The data that support the findings of this study are available from the corresponding author upon reasonable request.

References

1. A. Steinegger, O. S. Wolfbeis, and S. M. Borisov, "Optical Sensing and Imaging of pH Values: Spectroscopies, Materials, and Applications," *Chemical Reviews* 120, no. 22 (2020): 12357–12489.

2. M. T. Ghoneim, A. Nguyen, N. Dereje, et al., "Recent Progress in Electrochemical pH-Sensing Materials and Configurations for Biomedical Applications," *Chemical Reviews* 119, no. 8 (2019): 5248–5297.

3. S. L. Percival, S. M. MPhil, J. A. Hunt, and E. J. Woods, "The Effects of pH on Wound Healing, Biofilms, and Antimicrobial Efficacy," *Wound Repair and Regeneration* 22, no. 2 (2014): 174–186.

4. P. Sim, X. L. Strudwick, Y. M. Song, A. J. Cowin, and S. Garg, "Influence of Acidic pH on Wound Healing In Vivo: A Novel Perspective for Wound Treatment," *International Journal of Molecular Sciences* 23, no. 21 (2022): 13655.

5. J. Guo, Y. Cao, Q. Y. Wu, Y. M. Zhou, Y. H. Cao, and L. S. Cen, "Implications of pH and Ionic Environment in Chronic Diabetic Wounds: An Overlooked Perspective," *Clinical, Cosmetic and Investigational Dermatology* 17 (2024): 2669–2686.

6. F. Mariani, M. Serafini, I. Gualandi, et al., "Advanced Wound Dressing for Real-Time pH Monitoring," *ACS Sensors* 6, no. 6 (2021): 2366–2377.

7. C. Wang, E. S. Sani, C. D. Shih, et al., "Wound Management Materials and Technologies from Bench to Bedside and Beyond," *Nature Reviews Materials* 9, no. 8 (2024): 550–566.

8. X. Wang, J. Cheng, and H. Wang, "Chronic Wound Management: A Liquid Diode-Based Smart Bandage with Ultrasensitive pH Sensing Ability," *Microsystems & Nanoengineering* 10, no. 1 (2024): 193.

9. X. Zhu, H. Sun, B. Yu, et al., "A Flexible pH Sensor Based on Polyaniline@oily Polyurethane/Polypropylene Spunbonded Nonwoven Fabric," *RSC Advances* 14, no. 8 (2024): 5627–5637.

10. T. Nezakati, A. Seifalian, A. Tan, and A. M. Seifalian, "Conductive Polymers: Opportunities and Challenges in Biomedical Applications," *Chemical Reviews* 118, no. 14 (2018): 6766–6843.

11. Y. Li, Y. Mao, C. Xiao, X. Xu, and X. Li, "Flexible pH Sensor Based on a Conductive PANI Membrane for pH Monitoring," *RSC Advances* 10, no. 1 (2020): 21–28.

12. F. Mazzara, B. Patella, C. D'Agostino, et al., "PANI-Based Wearable Electrochemical Sensor for pH Sweat Monitoring," *Chemosensors* 9, no. 7 (2021): 169.

13. M. Beygisangchin, S. A. Rashid, S. Shafie, A. R. Sadrolhosseini, and H. N. Lim, "Preparations, Properties, and Applications of Polyaniline and Polyaniline Thin Films-A Review," *Polymers* 13, no. 12 (2021): 2003.

14. J. Wang and D. Zhang, "One-Dimensional Nanostructured Polyaniline: Syntheses, Morphology Controlling, Formation Mechanisms, New Features, and Applications," *Advances in Polymer Technology* 32, no. S1 (2013): E323–E368.

15. M. S. Hossain, N. Padmanathan, M. M. R. Badal, K. M. Razeeb, and M. Jamal, "Highly Sensitive Potentiometric pH Sensor Based on Polyaniline Modified Carbon Fiber Cloth for Food and Pharmaceutical Applications," *ACS Omega* 9, no. 38 (2024): 40122–40133.

16. Y. Zhao, Y. Yu, S. Zhao, R. Zhu, J. Zhao, and G. Cui, "Highly Sensitive pH Sensor Based on Flexible Polyaniline Matrix for Synchronal Sweat Monitoring," *Microchemical Journal* 185 (2023): 108092.

17. A. U. Svensby, E. Nygren, A. Gefen, et al., "The Importance of the Simulated Wound Fluid Composition and Properties in the Determination of the Fluid Handling Performance of Wound Dressings," *International Wound Journal* 21, no. 5 (2024): e14861.

18. Y. Bai, R. Zhu, J. Zhao, and G. Cui, "Super-Nernstian Model Based on Acid Doped Polyaniline pH Sensor," *Microchemical Journal* 203 (2024): 110715.

19. C. Zhu, H. Xue, H. Zhao, et al., "A Dual-Functional Polyaniline Film-Based Flexible Electrochemical Sensor for the Detection of pH and Lactate in Sweat of the Human Body," *Talanta* 242 (2022): 123289.

20. S. N. Kumar, F. Gaillard, G. Bouyssoux, and A. Sartre, "High-Resolution XPS Studies of Electrochemically Synthesized Conducting Polyaniline Films," *Synthetic Metals* 36, no. 1 (1990): 111–127.

21. F. Fenniche, Y. Khane, A. Henni, D. Aouf, and D. E. Djafri, "Synthesis and Characterization of PANI Nanofibers High-Performance Thin Films via Electrochemical Methods," *Results in Chemistry* 4 (2022): 100596.

22. V. Lyutov, V. Kabanova, O. Gribkova, A. Nekrasov, and V. Tsakova, "Electrochemically-Obtained Polysulfonic-Acids Doped Polyaniline Films-A Comparative Study by Electrochemical, Microgravimetric and XPS Methods," *Polymers* 12, no. 5 (2020): 1050.

23. W. Wang, F. Yang, C. Chen, L. Zhang, Y. Qin, and M. Knez, "Tuning the Conductivity of Polyaniline through Doping by Means of Single Precursor Vapor Phase Infiltration," *Advanced Materials Interfaces* 4, no. 4 (2017): 1600806.

24. F. Huerta, C. Quijada, F. Montilla, and E. Morallón, "Revisiting the Redox Transitions of Polyaniline. Semiquantitative Interpretation of Electrochemically Induced IR Bands," *Journal of Electroanalytical Chemistry* 897 (2021): 115593.

25. A. J. S. Ahammad, A. A. Mamun, T. Akter, M. A. Mamun, S. Faraezi, and F. Z. Monira, "Enzyme-Free Impedimetric Glucose Sensor Based on Gold Nanoparticles/Polyaniline Composite Film," *Journal of Solid State Electrochemistry* 20, no. 7 (2016): 1933–1939.

26. J. Zhang, X. Yu, W. Guo, et al., "Construction of Titanium Dioxide Nanorod/Graphite Microfiber Hybrid Electrodes for a High Performance Electrochemical Glucose Biosensor," *Nanoscale* 8, no. 17 (2016): 9382–9389.

27. H. Wang, J. Lin, and Z. X. Shen, "Polyaniline (PANi) Based Electrode Materials for Energy Storage and Conversion," *Journal of Science: Advanced Materials and Devices* 1, no. 3 (2016): 225–255.

28. Y. Wu, X. Gao, and Y. Li, "Electrochemical Sensors Based on Polyaniline Nanocomposites for Detecting Cd (II) in Wastewater," *International Journal of Electrochemical Science* 19, no. 3 (2024): 100519.

29. J. H. Yoon, S. B. Hong, S. O. Yun, et al., "High Performance Flexible pH Sensor Based on Polyaniline Nanopillar Array Electrode," *Journal of Colloid and Interface Science* 490 (2017): 53–58.

30. N. Abu-Thabit, Y. Umar, E. Ratemi, A. Ahmad, and F. A. Abuilaiwi, "A Flexible Optical pH Sensor Based on Polysulfone Membranes Coated with pH-Responsive Polyaniline Nanofibers," *Sensors* 16, no. 7 (2016): 986.

31. H. J. Park, J. H. Yoon, K. G. Lee, and B. G. Choi, "Potentiometric Performance of Flexible pH Sensor Based on Polyaniline Nanofiber Arrays," *Nano Convergence* 6, no. 1 (2019): 9.

32. T. Guinovart, G. Valdés-Ramírez, J. R. Windmiller, F. J. Andrade, and J. Wang, "Bandage-Based Wearable Potentiometric Sensor for Monitoring Wound pH," *Electroanalysis* 26, no. 6 (2014): 1345–1353.

Supporting Information

Additional supporting information can be found online in the Supporting Information section. **Supporting Fig. S1:** The SEM image of the gold-coated PI substrate showed a smooth and flat surface. **Supporting Fig. S2:** Raman spectrum of PANI modified electrode. The spectrum shows characteristic bands at 1404, 1483, and 1606 cm^{-1}, corresponding to the quinoid C—C, C═N, and C═C stretching vibrations, respectively. Additional bands at 1230 cm^{-1} (C—N stretching, benzenoid), 1166 cm^{-1} (in-plane C—H bending, quinoid), and 816 cm^{-1} (out-of-plane C—H bending) further confirm the coexistence of benzenoid and quinoid units in the polymer chain. **Supporting Fig. S3:** Mechanism of electrochemical polymerization of polyaniline.[18] (a) oxidation of the aniline monomer at the anode to form a primary cation radical; (b) coupling of two cation radicals followed by deprotonation and rearomatization to yield dimers; (c) further oxidative chain growth through the oxidation of dimers to

cation radicals and their subsequent reaction with additional monomer cation radicals; and (d) spontaneous doping of the resulting polymer chain, leading to the formation of the conductive doped form of PANI, which occurs uniquely in the electrochemical polymerization process. **Supporting Table S1:** Composition of the modified simulated wound fluid. **Supporting Table S2:** Summary of drift rates of the PANI electrode under two experimental conditions: (a) 24-hour continuous measurement and (b) measurement after 24-hour immersion. **Supporting Table S3:** Comparison of the performances of different pH sensors.